Water Science & Technology

IWA PUBLISHING



Water Science & Technology Vol 90 No 3, 1070 doi: 10.2166/wst.2024.255

# Alkalinity control in sludge propels the conversion of concrete slurry waste into micro- and nano-sized biogenic $CaCO_3$

Jinbo Zhao[a,b], Jiacheng Feng[a], Yifan Du[a], Zhiyang Yan[a], Xiaoguang Li[a], Jinyi Qin [a,b,*], Ming Su [b,c] and Min Yang [b,c]

[a] School of Civil Engineering, Chang'an University, Xi'an 710054, China
[b] State Key Laboratory of Environmental Aquatic Chemistry, Research Center for Eco-Environmental Sciences, Chinese Academy of Sciences, Beijing 100085, China
[c] University of Chinese Academy of Sciences, Beijing 100049, China
*Corresponding author. E-mail: jinyi.qin@chd.edu.cn

JQ, 0000-0001-5727-1846

## ABSTRACT

The utilization of *Bacillus sp.* for the production of bio-$CaCO_3$ in concrete crack repair and strength enhancement has attracted considerable attention. However, microbial-induced calcium carbonate precipitation (MICP) has yet to be explored as a precedent with activated sludge. Here calcium sourced from concrete slurry waste (CSW) and carbon from sludge microbial β-oxidation under alkaline were used to generate micro/nano $CaCO_3$. The results indicate that the main crystalline form of the generated precipitated particles is calcite, with a particle size ranging from 0.7 to 10 μm. Minimal heavy metals were found in the supernatant following settling. And at the optimum pH of 8.5–9, carbon capture reached 743 mg $L^{-1}$, and $CaCO_3$ production reached 1,191 mg $L^{-1}$, and dominant phylum were *Proteobacteria* and *Bacteroidota*, with *Thauera* being a prevalent genus adept in β-oxidation. Mass balance analysis showed that alkali promotes microbial β-oxidation of organisms to produce $CO_2$ and facilitate storage. Thus, the alkaline regulation of metabolism between microbe and CSW provides a novel way of sludge to initiate MICP.

**Key words:** calcite, concrete slurry waste, MICP, micro- and nano-sized biogenic $CaCO_3$, *Thauera*

## HIGHLIGHTS

- Utilizing concrete slurry waste as a calcium source and sludge β-oxidation as a carbon source can successfully produce bio-$CaCO_3$.
- pH 8.5–9 is the optimal alkaline control for *Thauera* to be the dominant genus undergoing β-oxidation to produce $CO_2$.
- Bio-$CaCO_3$ is a 0.7–10 μm calcite particle, which is an excellent material for repairing concrete.
- There is no risk of heavy metal leakage during operation.

## GRAPHICAL ABSTRACT

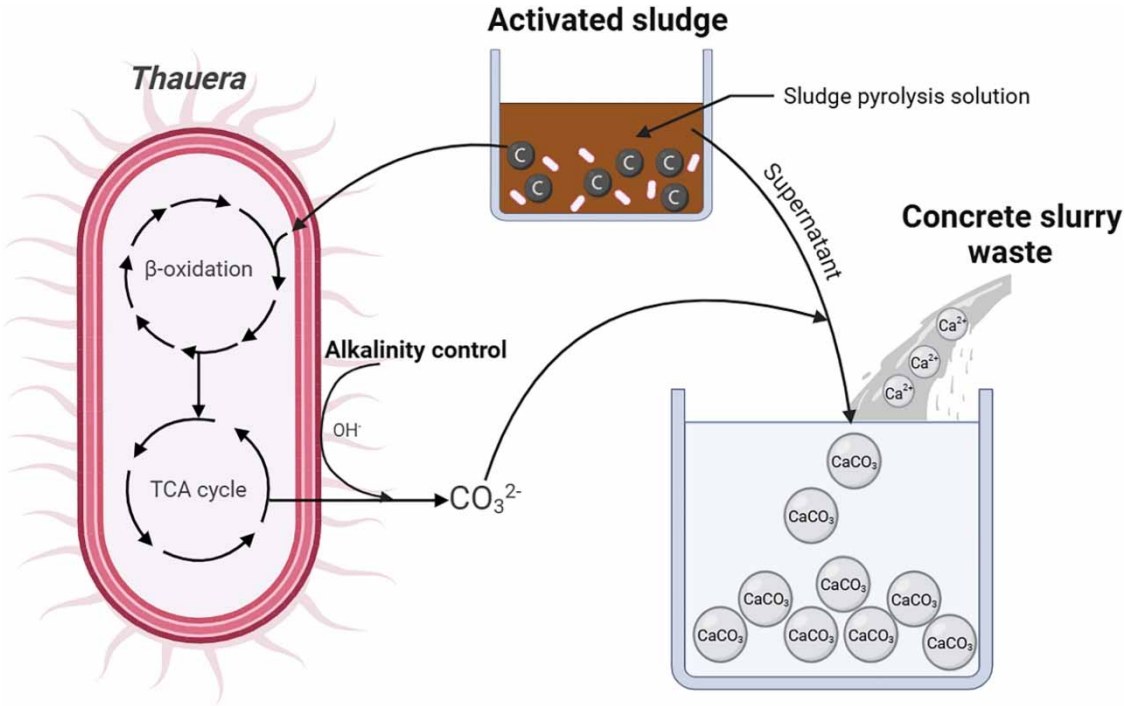


## 1. INTRODUCTION

During the concrete production process, a large amount of concrete slurry waste (CSW) is generated, attributed to the washing of concrete trucks, dust reduction, and sphere cleaning operations. Characterized by a pH level exceeding 11.5, CSW is rich in calcium silicate (Xuan *et al.* 2016). CSW is classified as a corrosive hazardous substance. If disposed of in landfills, it would cause detrimental effects on our surrounding environment and ecosystems due to its high pH value. In addition, sedimentation and post-treatment processes lead to the accumulation of waste slurry particles, contributing to dust pollution in the concrete production environment and overlooking the potential recycling and utilization of significant mineral resources. However, the Chinese national standard (GB/T 14902-2012) mandates the recycling of CSW. Previous research has demonstrated that *Bacillus* sp. can utilize calcium sources in concrete to synthesize $CaCO_3$ bio-nanoparticles, which are beneficial for repairing concrete cracks and filling pores (Qin *et al.* 2021b). Consequently, microbial-induced calcium carbonate precipitation (MICP) offers a viable alternative for the recycling of calcium resources in CSW.

CSW is recognized as a potential source of calcium carbonate. Upon introducing $CO_2$ into the aqueous phase, up to 30% of calcium can be extracted from CSW, yielding $CaCO_3$ with a purity exceeding 97% (Iizuka *et al.* 2012). However, $CO_2$′s low water solubility constrains $CaCO_3$ production (Hui *et al.* 2022). The adjustment of pH enhances $CO_2$ capture, promotes $CO_3^{2-}$ production, and facilitates the generation of abundant $CaCO_3$ nanoparticles. More importantly, bio-nano-$CaCO_3$, synthesized by urease-producing bacteria and enriched from waste-activated sludge via the MICP method, has various applications including repairing concrete voids, cementing soil, improving soil strength, and suppressing coal dust in coal mines (Yang *et al.* 2020; Liu *et al.* 2022). Utilizing urease-producing bacteria to produce micro- and nano-$CaCO_3$ from carbonized sludge and urine for the production of sustainable bio-cement has been explored (Yang *et al.* 2022). The use of *Bacillus pasteurii* to produce bio-$CaCO_3$ has been demonstrated to enhance the strength of expansive soils (Tian *et al.* 2022). *Sporosarcina ureilytica* ML-2 produces bio-$CaCO_3$ for treating waste sludge and immobilizing heavy metals (Zeng *et al.* 2023). Nonetheless, it is important to consider that using a single strain and adding calcium sources and urea to generate bio-$CaCO_3$ can significantly increase the costs involved. Breaking down urea can lead to the excessive production and accumulation of ammonia nitrogen, which, in turn, can acidify the water and promote eutrophication (Kumar *et al.* 2023). There remains a lack of direct research on producing micro- and nano-sized biogenic $CaCO_3$ (bio-$CaCO_3$) using microbial communities from activated

sludge and CSW. The biological metabolic mechanisms underlying MICP for nanoparticle production in CSW are not well understood, particularly the impact of pH on biochemical reaction pathways and alkalinity regulation.

For this, a comprehensive investigation was conducted on the system that harnesses CSW as a valuable resource through the bio-metabolism process of activated sludge. Additionally, the impact of pH on the efficiency of carbon capture and the production of $CaCO_3$ was thoroughly examined. At varying pH levels, analyses were conducted based on the bacterial community structure, the relative cell count, and the proportions of polysaccharides and proteins produced. Scanning electron microscopy (SEM) was used to determine the particle size, while X-ray diffraction (XRD) was used to identify the composition and crystalline form of the products. Inductively coupled plasma mass spectrometry (ICP-MS) was employed to verify the heavy metal residues in the supernatant following sludge settling and $CaCO_3$ precipitates. These findings offer novel insights into the recycling of CSW calcium resources and the generation of bio-$CaCO_3$, potentially benefiting the early strength of concrete.

## 2. MATERIALS AND METHODS

### 2.1. Materials

CSW was obtained from Shaanxi Future Venture Construction Technology Co., Ltd, Xi'an and stored at 4°C before use. Sludge, possessing an 80% moisture content, was procured from the No. 4 Wastewater Treatment Plant (WWTP). Chemical reagents for the experiments were procured from Sigma-Aldrich (MO, USA). $Ca^{2+}$, pH, suspended solids (SS), and chemical oxygen demand (COD) were determined according to the following national standards (GB7476-1987), (GB11901-89) and (HJ828-2017). Results are presented in Table 1.

### 2.2. Preparation of carbon source for sludge pyrolysis solution

To better adapt microbes to the carbon source in actual wastewater, the hydrothermal pretreatment of sludge organisms was employed as a simulated carbon source. This process breaks down lipids into long-chain fatty acids and volatile fatty acids, and proteins into ammonia and volatile fatty acids (Qin *et al.* 2021c). There is minimal degradation of long-chain fatty acids in sludge subjected to 90 °C hydrolysis (Charuwat *et al.* 2018). Consequently, Table 1 shows the biochemical oxygen demand ($BOD_5$) and COD during pyrolysis for 1 h at a pH of 11 and a temperature of 90 °C. The $BOD_5$/COD ratio exceeding 0.6 indicates its bioavailability.

### 2.3. Operation of the bio-$CaCO_3$ generation reactor

About 4 L of sludge microbes were introduced into an 8 L reactor. Intermittent aeration was performed at a rate of 7 L $min^{-1}$ to maintain dissolved oxygen levels between 2 and 5 mg $L^{-1}$. Mechanical stirring ensures the uniform distribution of sludge in the reactor. Furthermore, an automatic NaOH syringe pump was utilized to maintain an alkaline pH. The reactor is placed in a water bath system to ensure that a consistent temperature of 25 °C is maintained. Sludge pyrolysate was added to maintain an input COD of 300 mg $L^{-1}$. The reaction cycle spanned 24 h, comprising 23 h of aerobic reaction. After that, there was 30 min of settling and the supernatant was then combined with CSW to produce nanoparticles, followed by 30 min dedicated to $CaCO_3$ nanoparticle generation. The nanoparticle precipitates were enriched through centrifugation, with the supernatant subsequently discarded. The enriched precipitates were then dried and weighed. After the aerobic reaction, the supernatant following sludge settling was collected, and here $CO_3^{2-}$ and $HCO_3^-$ content were analyzed adhering to standards (DZ/T 0064.49–2021). Heavy metals, such as Cr, Cu, Zn, Cd and Pb, were measured in the supernatant following sludge settling and $CaCO_3$ precipitates using ICP-MS (Thermo Fisher iCPA Q USA). Before measurement, the samples undergo acid dissolution treatment. In addition, to fully utilize the CSW and reduce operating costs, a reflux experiment was set up, which differs from the former in that the CSW reflux reactor, after generating calcium carbonate, provides alkalinity.

**Table 1** | Characteristics of CSW and the bioavailability of sludge pyrolysates

| CSW (mg $L^{-1}$) | | | | Sludge pyrolysates (mg $L^{-1}$) | | |
|---|---|---|---|---|---|---|
| pH | $Ca^{2+}$ | SS | COD | COD | $BOD_5$ | $BOD_5$/ COD |
| 12–13.5 | 747.09 | 6,745 | 68 | 7,300 ± 100 | 4,492.5 ± 3.5 | 0.62 ± 0.005 |

The generated nanoparticles were analyzed using SEM (SU-8082, Japan) to assess their structure and particle size. XRD analysis (Ultima IV, Japan) was employed to determine the composition and crystalline structure of the nanoparticles. Next-generation sequencing based on 16S rRNA was utilized to analyze the microbial community structure. Sludge microorganisms with pH ranges of 7.5–8.0, 8.5–9.0, and 9.5–10.0 were entrusted to Beijing Kinko Biotechnology Co for testing.

### 2.4. Fluorescence observation of proteins and polysaccharides in dyed sludge

The sludge was immersed in 10 g $L^{-1}$ of fluorescein isothiocyanate isomer I (FITC) to stain proteins, then in 0.1 g $L^{-1}$ of concanavalin A-alexa fluor (Con A) to label polysaccharides, and in 1 mg $L^{-1}$ of 4,6-diamidino-2-phenylindole dihydrochloride (DAPI) to stain nucleic acids. Staining of the sludge was conducted by methodologies previously described (Chen *et al.* 2007; Yang *et al.* 2023). Subsequently, the samples were paraffin-embedded, sectioned using a microtome (Leica RM2126RT, Germany), and examined and imaged with a fluorescence microscope (Olympus BX61 + DP72, Japan). The excitation wavelengths for Con A, FITC, and DAPI were 555, 488, and 358 nm, respectively.

To confirm the reproducibility of the experimental results, all experiments were performed in triplicate. The graphs were drawn using Origin (OriginLab, USA, 2018). Values are expressed as mean values ± standard deviations. Image J (NIH, USA) was utilized to calculate the fluorescence area.

## 3. RESULTS AND DISCUSSION

### 3.1. Effect of pH adjustment on carbon capture effectiveness and bio-$CaCO_3$ output

In alkaline water, $CO_2$ simultaneously exists in the forms of $CO_3^{2-}$ and $HCO_3^-$ (Qin *et al.* 2021a). With an increase in pH, $HCO_3^-$ progressively converts into $CO_3^{2-}$. Conversely, with a decrease in pH, $CO_3^{2-}$ progressively transforms into $HCO_3^-$, subsequently forming $H_2CO_3$ molecules. $H_2CO_3$, due to its instability, readily decomposes into $H_2O$ and $CO_2$, subsequently escaping into the air. Consequently, pH plays a pivotal role in determining the efficiency of carbon capture. As illustrated in Figure 1 at a pH of 7.5–8, $CO_2$ is present exclusively in the form of $HCO_3^-$, reaching a maximum concentration of 250 mg $L^{-1}$. During this phase, a considerable volume of $CO_2$, generated via microbial β-oxidation, is released from the water into the air. Upon the pH reaching 8.5–9, $CO_2$ continues to coexist in the forms of $CO_3^{2-}$ and $HCO_3^-$. The combined concentration of $CO_3^{2-}$ and $HCO_3^-$ (carbon capture effectiveness) experiences rapid growth over 3 days, eventually stabilizing at 700–800 mg $L^{-1}$. At pH ranging from 9.5 to 10, the carbon capture effectiveness can ultimately stabilize at approximately 1,000 mg $L^{-1}$. During the pH elevation from 7.5–8 to 8.5–9 and subsequently to 9.5–10, the carbon capture effectiveness escalates by 193.7 and 34.6%, respectively. The maximum yield of $CaCO_3$ rises from 415.8 to 1,190.7 mg $L^{-1}$ and subsequently to 1,649.3 mg $L^{-1}$, representing an increase of 186.3 and 38.5%, respectively. This suggests that the growth rate of the carbon capture effectiveness and the yield of bio-$CaCO_3$ are significantly higher at a pH of 8.5–9 than at a pH of 9.5–10. Typically, for aerobic biological treatment, the pH is recommended to be between 6 and 9. An overly elevated pH can result in the death of some microorganisms, extend the adaptation period, or potentially inhibit microbial activity. Furthermore, with increasing pH, the supernatant of the reactor becomes increasingly turbid, adversely affecting the purity of the produced $CaCO_3$. Moreover, a higher pH entails increased operational costs, and therefore, establishing a pH level of 8.5–9 is considered the optimal alkaline condition for producing bio-$CaCO_3$.

As illustrated in Table 2, following the carbon source calculation resulting from the transformation of sewage organics into $CO_2$, a mass balance pertaining to carbon transformation and capture has been established in reactors with a pH of 9.5–10. The conversion ratio of COD to $CO_2$ has been derived from the existing literature (Bao *et al.* 2015). During this process, the $CO_2$ concentration supplemented by air in aerobic aeration amounts to 1,467.79 mg $L^{-1}$, markedly surpassing the carbon capture quantity of 148.63 mg $L^{-1}$ in the control water and 726.31 mg $L^{-1}$ in the bio-$CaCO_3$ generation reactor. This demonstrates that a substantial portion of the $CO_2$ entering the reactor during the aeration is released into the air. Additionally, the carbon capture quantity in the reactor exceeds the combined carbon of the control water and the incoming source. This implies that the alkali addition not only enhances the conversion of nearly all soluble COD into $CO_2$ via bio-metabolism but also aids in dissolving some insoluble COD in the sludge pyrolysate, thereby enabling more efficient utilization by microbial aerobic respiration. In addition, an alkaline environment favors carbon capture. The alkali addition facilitates microbial carbon transformation, leading to $CO_2$ production, which is advantageous for storing the generated $CO_2$ in water.

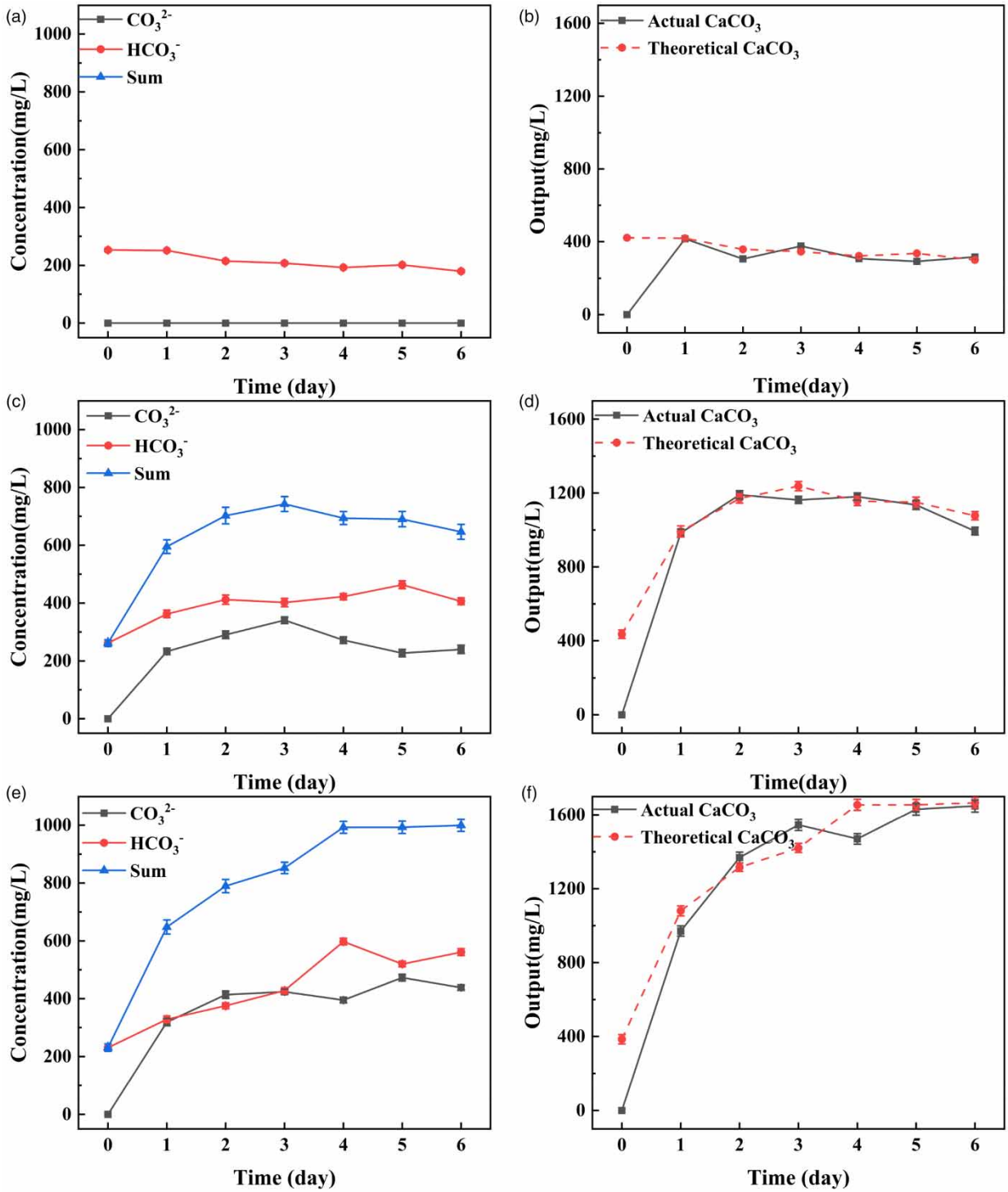


**Figure 1** | Effect of pH 7.5–8 (a and b), 8.5–9 (c and d), and 9.5–10 (e and f) on carbon capture's effectiveness and bio-$CaCO_3$ output (green for theoretical and orange for actual output).

### 3.2. The impact of reactor operational ways on carbon capture efficiency and bio-$CaCO_3$ output

Owing to the high alkalinity of CSW, which exhibits a pH of 12–13.5 (Xuan *et al.* 2016), its return to the reactor following $CaCO_3$ production can offer an alkaline environment, facilitating waste resource utilization and diminishing the operational costs of the reactor. As depicted in Figure 2(a) and 2(c), with pH levels of 8.5–9, the carbon capture effectiveness stabilized

**Table 2** | Carbon mass balance in the bio-$CaCO_3$ generation reactor

| Carbon of incoming | Carbon of aeration | Carbon capture in control water | Carbon capture in reactor |
|---|---|---|---|
| | | mg $L^{-1}$ | |
| 291 ± 5.8 | 1,467.79 ± 23.82 | 148.63 ± 2.78 | 726.31 ± 8.75 |

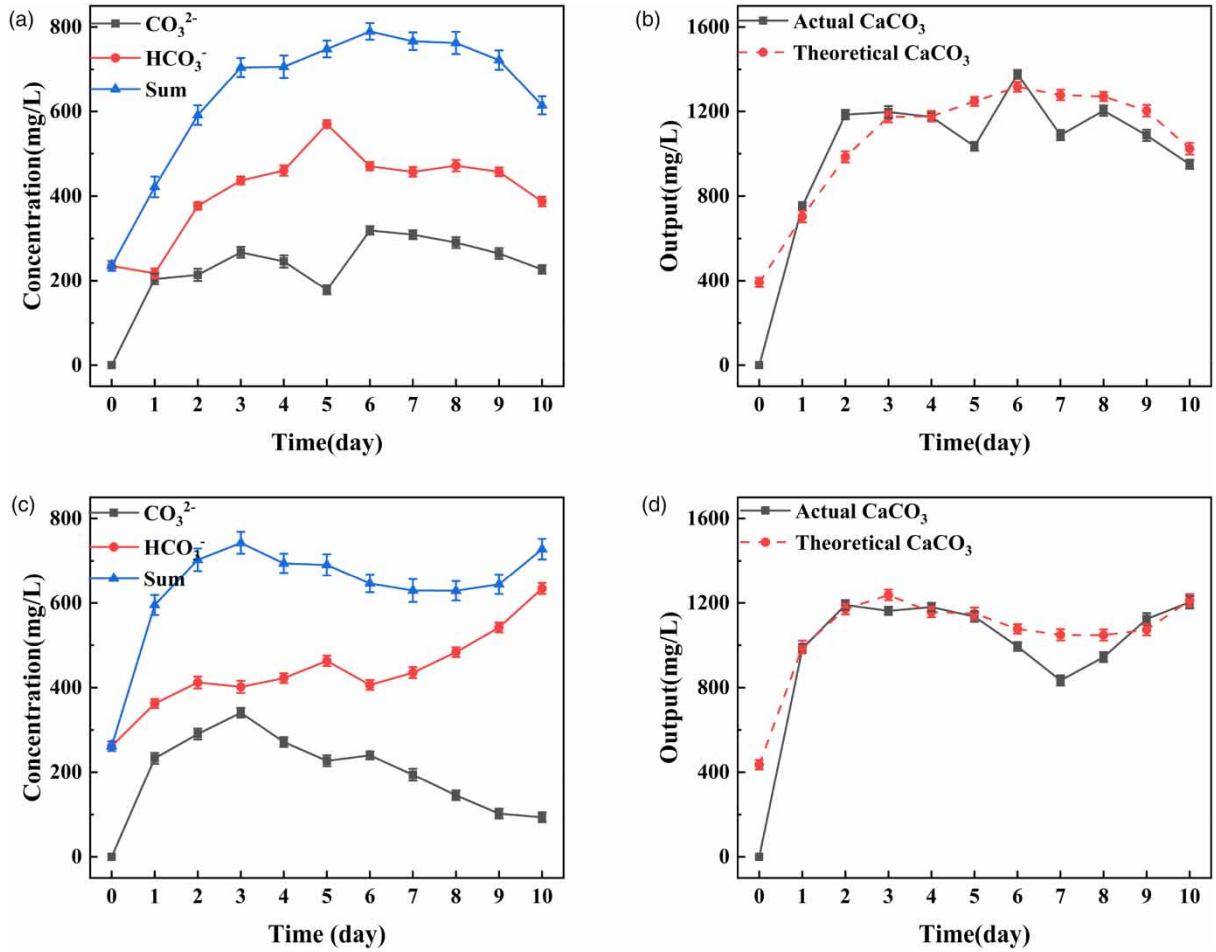


**Figure 2** | Effect of reflux (a and b) and no-reflux (c and d) way on carbon capture and bio-$CaCO_3$ output (green for theoretical and orange for actual output).

between 700 and 800 mg $L^{-1}$ following 3 days of rapid increase. In the no-reflux approach, carbon capture effectiveness nearly peaked at 702.5 mg $L^{-1}$ on the 2nd day, in contrast to a near peak of 742.6 mg $L^{-1}$, while reflux reached only 591.2 mg $L^{-1}$, suggesting a more expedited startup period. During days 3–8, reflux progressively increased from 704.3 mg $L^{-1}$ to a maximum of 789.7 mg $L^{-1}$. This increase is attributed to the additional minor carbon source from the reflux CSW (refer to Table 1), while the subsequent decline in carbon capture effectiveness is likely due to the inhibition of cellular respiration from accumulated heavy metals and salts (Hong *et al.* 2013; Ma *et al.* 2015; He *et al.* 2017). In the no-reflux reactor depicted in Figure 2(c), carbon capture effectiveness reached its apex at 742.58 mg $L^{-1}$ on the 3rd day. Despite a minor decline from days 4 to 10, it remained relatively stable at 650–750 mg $L^{-1}$, marginally lower than the reflux reactor. Figure 2(b) and 2(d) illustrates that under reflux and no-reflux operation way, the peak production of bio-$CaCO_3$ was 1,376.4 and 1,204 mg $L^{-1}$, respectively, aligning closely with theoretical projections. Reflux's CSW does not impact the efficiency of carbon capture or the production of bio-$CaCO_3$. In addition, Figure 2(a) and 2(c) exhibits distinct peaks in $HCO_3^-$ levels and corresponding valleys in $CO_3^{2-}$ levels on day 5. This observed trend can be attributed to the bulking

of sludge that occurred around day 5, coinciding with a sludge settling velocity of approximately 90% (refer to Figure S5). Consequently, certain microorganisms present in the bulking sludge experienced mortality in the highly alkaline environment, leading to the leaching of intracellular lipids. These lipids were subsequently converted into fatty acids (Wilson & Novak 2009), thereby contributing to the reduction in pH levels. Moreover, this conversion process also served as an additional carbon source for the system. In summary, for effective pH adjustment of the reactor and reduced operational costs, the adoption of the CSW reflux way is recommended, as it is more conducive to the production of bio-$CaCO_3$.

### 3.3. Effect of pH on the distribution of microbial polysaccharides and proteins

pH exerts a significant influence on the protein and polysaccharide content in microorganisms (Yu *et al.* 2017). As evidenced in Figure 3, with an increase in pH, the absolute value of nucleic acids in the sludge microbial community rises, signifying a rise in microbial quantity. Under the premise that all samples have the same cell number in the field of view; to illustrate the relative content changes of proteins and polysaccharides, we utilized the fluorescence area of nucleic acids as a reference (blue). With an increase in pH, the area of nucleic acid continuously approaches 3,600 $\mu m^2$ at pH 9.5–10, while the area occupied by proteins and polysaccharides both increased and then decreased, reaching approximately 2,100 $\mu m^2$ at pH 8.5–9. The relative ratio of protein declines from 0.74 to 0.70 and ultimately to 0.52. This phenomenon may be attributed to β-oxidation of proteins, as the degradation of proteins into amino acids, subsequent deamination and decarboxylation, facilitates the formation of fatty acids that undergo β-oxidation. Conversely, the relative ratio of polysaccharides escalates from 0.42 to 0.72 with an increase in pH, subsequently decreasing to 0.49. The increase in polysaccharide content from pH 7.5–8 to 8.5–9 is attributed to the secretion of polysaccharides by microorganisms in response to the alkaline environment (Yu *et al.* 2017). Further increase in pH reduces the relative ratio of polysaccharides to 0.49, but it remains higher than 0.42 at pH 7.5–8. This could be due to the increased solubility of polysaccharides at higher alkalinity (Wang *et al.* 2022). In summary, as pH increases, the absolute value of nucleic acids in the sludge microbial community escalates, signifying a rise in microbial quantity. However, the relative ratio of protein per microorganism decreases, suggesting that β-oxidation metabolism of proteins occurs. The relative ratio of polysaccharides increases initially and then decreases. This increase occurs in response to the unfavorable environment at pH 8.5–9.

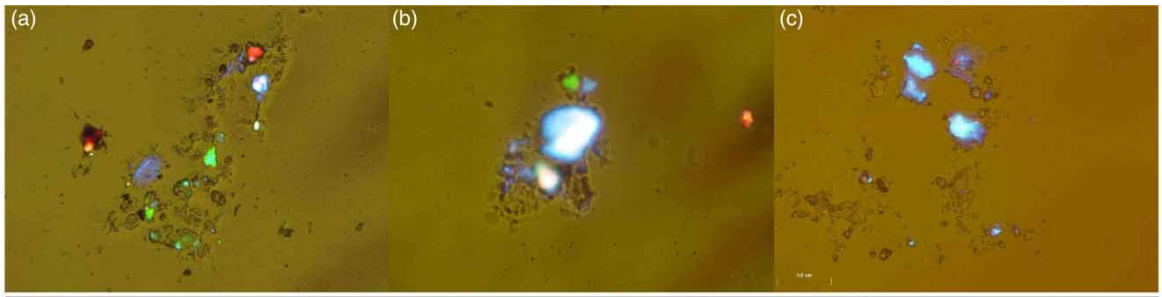


| pH | The occupied area in the field of view ($\mu m^2$) | | | Relatively ratio | |
|---|---|---|---|---|---|
| | Protein ($A_{Pro}$) | Polysaccharide ($A_{Sac}$) | Nucleic acid ($A_{Nuc}$) | $A_{Sac}/A_{Nuc}$ | $A_{Pro}/A_{Nuc}$ |
| 7.5-8 | 1728 ± 37.38 | 978 ± 23.75 | 2329 ± 25.45 | 0.42 | 0.74 |
| 8.5-9 | 2134 ± 44.22 | 2193 ± 39.67 | 3040 ± 65.86 | 0.72 | 0.70 |
| 9.5-10 | 1883 ± 29.76 | 1758 ± 50.22 | 3603 ± 68.79 | 0.49 | 0.52 |

**Figure 3** | Effect of pH 7.5–8 (a), 8.5–9 (b), and 9.5–10 (c) on the distribution of microbial polysaccharides (red) and protein (green) composition.

### 3.4. Analysis of the microbial community structure of sludge at different pH levels

As depicted in Figure 4, at the phylum level, *Proteobacteria*, *Bacteroidota*, *Patescibacteria*, and *Acidobacteriota* emerge as dominant. With the increase in pH, the relative abundance of *Proteobacteria* consistently escalates from 47.29 to 77.20%, illustrating its adaptability to an alkaline environment. As the pH progresses from 7 to 9, *Bacteroidota's* relative abundance increases from 10 to 34%. Nevertheless, upon reaching a pH value of 10, its relative abundance diminishes to 14%. While *Bacteroidota* can thrive in mildly alkaline conditions at pH 9, it is intolerant to environments that exceed a pH of 9.5. *Patescibacteria* and *Acidobacteriota* exhibit a consistent decline in relative abundance with pH elevation, decreasing by 11 and 5%, respectively. At the genus level, *Thauera* dominates at pH 8.5–9, while *Brevundimonas* prevails at pH 10, with peak relative abundances of 14 and 16%, respectively. *Thauera* bacteria, which are prevalent in diverse wastewater denitrification systems, facilitate the removal of nitrogen and phosphorus through denitrification. With the pH elevation from 9 to 10, *Thauera's* relative abundance diminishes from a leading 14–7%, reflecting its preference for moderately alkaline rather than highly alkaline conditions. Furthermore, *Thauera* is capable of producing polyhydroxyalkanoate facilitated by the acetyl coenzyme A gene (Andreolli *et al.* 2022; Raunhan *et al.* 2023), establishing it as a key genus in β-oxidation at pH 8.5–9. *Zoogloea* is critical for the settling performance of activated sludge (An *et al.* 2016). The absence of *Zoogloea* in environments with pH levels ranging from 8.5 to 9 and 9.5 to 10 poses some inconvenience in the production of bio-$CaCO_3$. In conclusion, *Proteobacteria* and *Bacteroidota*, at the phylum level, are predominant in bio-$CaCO_3$ production, while, at the genus level, *Thauera*, proficient in *β*-oxidation, excels in bio-$CaCO_3$ production at pH 8.5–9. Correspondingly, *Zoogloea's* limited viability in alkaline results in ineffective sludge settling and turbid supernatant.

### 3.5. Analysis of bio-$CaCO_3$ using SEM and XRD

Figure 5 illustrates that bio-$CaCO_3$ predominantly exhibits a sphere shape, with diameters predominantly in the 0.7–10 μm range, to some extent to the nanometer scale. Owing to their diminutive size, these micro-/nano-sized calcium carbonate particles demonstrate superior dispersibility, markedly enhancing the potential for crosslinking with other materials (Boyjoo *et al.* 2014). Consequently, micro-/nano-sized calcite-type calcium carbonate emerges as an exemplary material for repairing concrete cracks and augmenting its mechanical properties (Cui *et al.* 2021). $CaCO_3$ exists in three crystalline forms: calcite, aragonite, and vaterite, with calcite being the most thermodynamically stable. Furthermore, its considerable strength facilitates compatibility with cementitious materials. Figure 5(c) depicts an XRD analysis of the products that are predominantly composed of calcite $CaCO_3$, with trace amounts of $Al_1Si_{143}N_{191}O_1$ and KCl. $Al_1Si_{143}N_{191}O_1$ is likely derived from cement and its hydration products, whereas $Cl^-$ is sourced from the dilute hydrochloric acid utilized for pH adjustment in the CSW. Similar to cement, calcite $CaCO_3$ boasts effective sand consolidation properties, and its non-permeable calcite layer offers corrosion protection for steel reinforcement (Ramachandran *et al.* 2001; Achal *et al.* 2013; Iswarya & Adalarasan 2020). In conclusion, the synthesized micro-/nano-sized $CaCO_3$ crystals, which are calcite type and highly pure, are well suited for use as concrete repair and reinforcement materials.

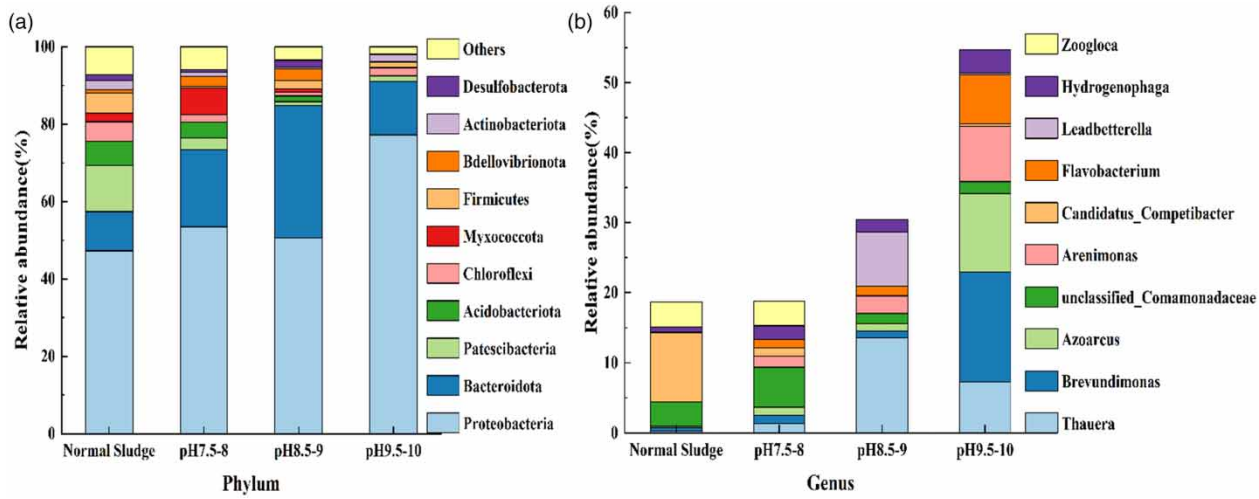


**Figure 4** | Different pH impact on the microbial communities at the phylum (a) and genus (b) level.

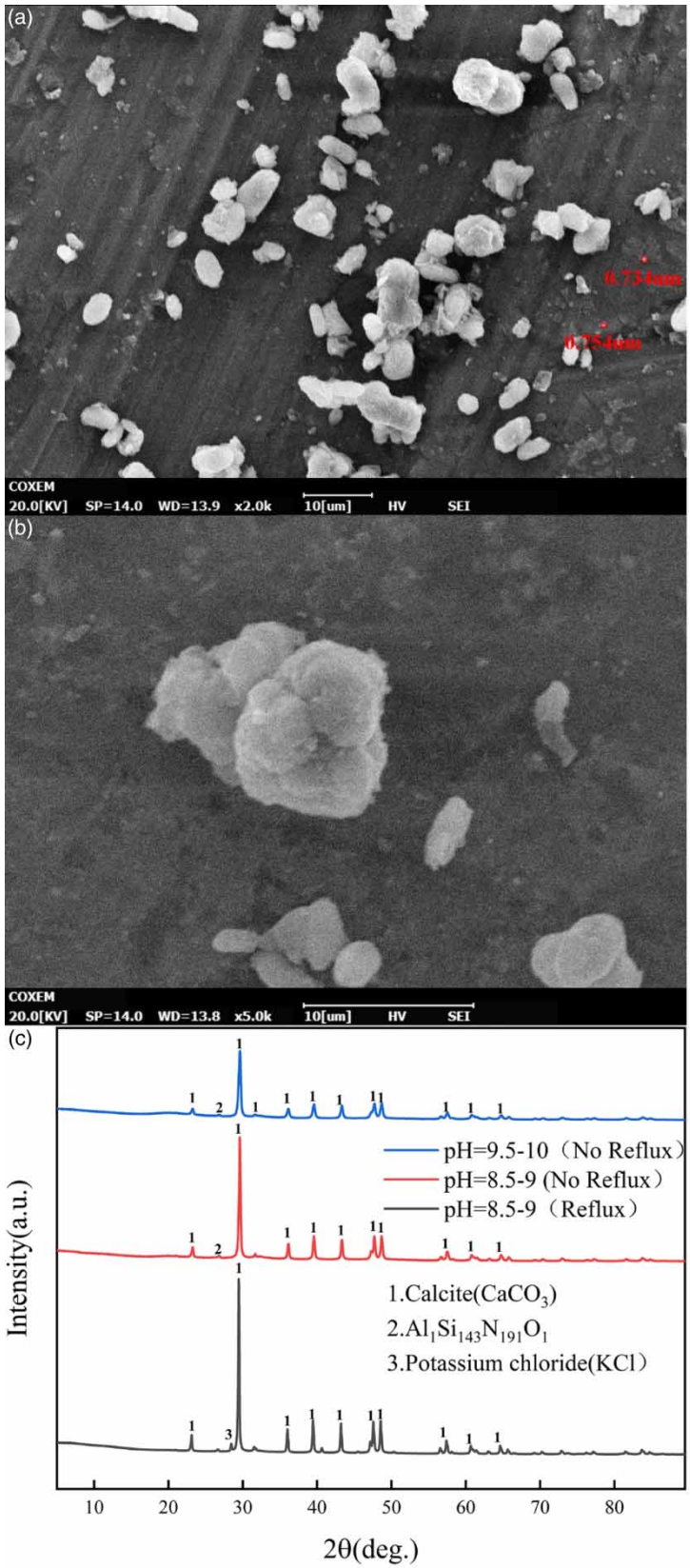


**Figure 5** | SEM analysis (5,000× for (a) and 10,000× for (b)) and XRD characterization of bio-$CaCO_3$ (c).

**Table 3** | Analysis of residue metal in the supernatant after bio-$CaCO_3$ generation

| | | Cr | Cu | Zn | Cd | Pb |
|---|---|---|---|---|---|---|
| Reflux (μg $L^{-1}$) | | | | | | |
| 9th day | After sludge settling | 0.88 ± 0.02 | 36.58 ± 0.74 | 5.87 ± 0.23 | 0.15 ± 0.01 | 0.24 ± 0.03 |
| | After $CaCO_3$ precipitation | 3.33 ± 0.09 | 21.71 ± 2.38 | 0.05 | 0.14 ± 0.28 | 0.43 ± 0.27 |
| 10th day | After sludge settling | 1.01 ± 0.78 | 53.51 ± 3.75 | 5.31 ± 0.55 | 0.12 ± 0.09 | 0.13 ± 0.02 |
| | After $CaCO_3$ precipitation | 2.85 ± 0.45 | 19.10 ± 2.34 | 0.05 | 0.17 ± 0.08 | 0.50 ± 0.24 |
| No reflux (μg $L^{-1}$) | | | | | | |
| 9th day | After sludge settling | 0.05 | 36.2 ± 3.48 | 17.4 ± 2.65 | 0.05 | 0.05 |
| | After $CaCO_3$ precipitation | 0.05 | 35.3 ± 2.27 | 10.4 ± 0.94 | 0.05 | 0.05 |

### 3.6. Assessment of heavy metal leaching after sludge settling and $CaCO_3$ precipitation

Activated sludge is known to contain heavy metals such as Pb, Cr, Cd, Ni, Zn, and Cu (Dewil *et al.* 2007), while CSW may accumulate Pb, Cr, and Cd (Xuan *et al.* 2016). Consequently, assessing the risk of heavy metal leaching during the reactor operation is crucial. Given that activated sludge can immobilize heavy metals, mainly through adsorption from surface functional groups, most residual heavy metals in CSW are likely to be adsorbed by the sludge and eliminated through sedimentation and discharge (Commenges-Bernole & Marguerie 2008; Ramrakhiani *et al.* 2016; Zhou *et al.* 2016). ICP-MS analysis (Table 3) reveals negligible amounts of Cr, Cd, and Pb in the supernatant following sludge settling in the no-reflux way, with Zn below 20 μg $L^{-1}$ and Cu at 36.20 μg $L^{-1}$. These low concentrations of metal ions should be absorbed by the sludge microbes and removed from the reactor by increasing the hydraulic retention time (HRT) and reducing the sludge retention time (SRT). In the reflux way, concentrations of Cr, Cd, and Pb following sludge settling are negligible in the supernatant. Post-day 9, Zn levels in the supernatant following $CaCO_3$ precipitation drop to just 0.05 μg $L^{-1}$. A contrast to 5.59 ± 0.28 μg $L^{-1}$, seen following sludge settling, suggests minimal Zn incorporation into bio-$CaCO_3$. The supernatant after sludge settling still contains a significant concentration of Cu, with levels reaching as high as 53.51 μg $L^{-1}$. It is worth noting that this concentration falls significantly below the groundwater quality standard (GB/T 14848-2017) stipulated by the Chinese national standard. However, the concentration of Cu in the supernatant significantly decreases to only 19.10 μg $L^{-1}$ after $CaCO_3$ precipitation. These findings indicate a limited uptake of Cu into the bio-$CaCO_3$. This could be attributed to the mixing of CSW and sludge supernatant in approximately a 1:1 ratio during the production process of $CaCO_3$, resulting in the Cu concentration in the supernatant after $CaCO_3$ precipitation being approximately half that present in the supernatant after sludge settling. Based on this, it can be inferred that the mobility of Cu bound within the activated sludge solution is restricted.

Furthermore, the supernatant following $CaCO_3$ precipitation in the reflux way contained slightly more heavy metals than that in the no-reflux way. This increase is potentially attributed to the salt accumulation within microbial cells due to the reflux of the supernatant in the reactor, which inhibits biological activity and diminishes the subsequent adsorptive ability of heavy metals (Hong *et al.* 2013; He *et al.* 2017). Nevertheless, these heavy metal concentrations remain well below the thresholds established by the comprehensive sewage discharge standard (GB8978-1996). In summary, the reflux way results in concentrations of Cr, Cd, and Pb in the supernatant that are below 3 μg $L^{-1}$, while Cu and Zn are somewhat higher, reaching maximum values of 53.51 and 17.4 μg $L^{-1}$, respectively. By increasing the HRT and reducing the SRT, these heavy metals can be primarily concentrated within the sludge microbes and effectively removed from the system.

## 4. CONCLUSION

Utilizing CSW as a calcium source and sludge β-oxidation products as a carbon source enabled the successful production of bio-$CaCO_3$ under alkaline conditions. The sludge pyrolysate, as a simulated COD, has a $BOD_5$/COD ratio that exceeds 0.6 with good biodegradability.

The ideal pH for $CaCO_3$ production was determined to be 8.5–9, achieving a maximum carbon capture of 742.6 mg $L^{-1}$ and a $CaCO_3$ yield of up to 1,190.7 mg $L^{-1}$. Mass balance analysis indicated that the addition of alkali enhances microbial β-oxidation, which degrades COD to produce $CO_2$ and aids in $CO_2$ storage. In addition, the reflux of supernatant in the reactor, providing an alkalinity environment and reducing costs, is recommended. As the pH value increases, the number of

microorganisms increases. Concurrently, a decrease in the relative protein content per microorganism was observed, suggesting that protein plays an important role in β-oxidation. Here, polysaccharides initially increase the relative content, followed by a decrease, with the elevation at pH 8.5–9, which serves as an adaptive response to adverse conditions. Simultaneously, *Proteobacteria* and *Bacteroidota* emerge as dominant phyla, with *Thauera* being a prevalent genus adept in β-oxidation. SEM disclosed that the majority of $CaCO_3$ precipitate particles exhibit a sphere shape, with a size of 0.7–10 μm in the range. XRD analysis demonstrated that the primary crystalline form of the precipitate is calcite. ICP-MS analysis indicated minimal heavy metal in the supernatant following sludge setting, and these trace heavy metals could be further removed by sludge discharge.

This methodology presents a novel strategy for waste sludge minimization, CSW reclamation, and the generation of bio-$CaCO_3$. The micro-/nano-bio-$CaCO_3$ production has a promising future, which can be used for concrete crack repair and strength enhancement. The discovery of alkaline regulation has expanded the application of MICP in CSW. Nevertheless, as there may be residual organic matter in the production process of bio-$CaCO_3$, further investigation is warranted to confirm the durability and mechanical properties of concrete integrated with this form of $CaCO_3$. The new operation should involve feeding a small amount of CSW into the reactor to maintain pH and continuously produce bio-$CaCO_3$ for slurry recharge in concrete. Furthermore, it is important to investigate whether the existing $CaCO_3$ in the CSW may agglomerate during prolonged placement, which will influence the particle size of MICP bio-$CaCO_3$.

## ACKNOWLEDGEMENTS

This work was financially supported by the Natural Science Foundation of China (Grant No. 51808044) and the Qinchuangyuan 'Scientist + Engineer' Team Construction Project of Shaanxi Province (2022KXJ-119). Supplementary data associated with this article can be found in the online version.

## AUTHOR CONTRIBUTIONS

Jinbo Zhao: conceptualization, writing – original draft, writing – review and editing, methodology, software. Jiacheng Feng: data curation, writing – review and editing, methodology, visualization. Yifan Du: formal analysis, investigation, writing – review and editing. Zhiyang Yan: methodology, supervision, resources, writing – review and editing. Xiaoguang Li: conceptualization, project administration, writing – review and editing. Jinyi Qin: conceptualization, validation, funding acquisition, project administration, resources. Ming Su: supervision, validation. Min Yang: supervision, writing – review and editing.

## DATA AVAILABILITY STATEMENT

Data cannot be made publicly available; readers should contact the corresponding author for details.

## CONFLICT OF INTEREST

The authors declare there is no conflict.

## REFERENCES

Achal, V., Mukerjee, A. & Reddy, M. S. 2013 Biogenic treatment improves the durability and remediates the cracks of concrete structures. *Construction and Building Materials* **48**, 1–5.

An, W., Gao, N., Xia, M., Dai, J., Yu, D. & Qiu, D. 2016 Physiological characteristics and systematic classification of the Zoogloea species and their role in the activated sludge. *Chinese Journal of Applied and Environmental Biology* **22**, 1167–1174.

Andreolli, M., Scerbacov, V., Frison, N., Zaccone, C. & Lampis, S. 2022 *Thauera* sp. Sel9, a new bacterial strain for polyhydroxyalkanoates production from volatile fatty acids. *New Biotechnology* **72**, 71–79.

Bao, Z., Sun, S. & Sun, D. 2015 Characteristics of direct $CO_2$ emissions in four full-scale wastewater treatment plants. *Desalination and Water Treatment* **54**, 1070–1079.

Boyjoo, Y., Pareek, V. K. & Liu, J. 2014 Synthesis of micro and nano-sized calcium carbonate particles and their applications. *Journal of Materials Chemistry A* **2**, 14270–14288.

Charuwat, P., Boardman, G., Bott, C. & Novak, J. T. 2018 Thermal degradation of long chain fatty acids: Charuwat *et al.* *Water Environment Research* **90**, 278–287.

Chen, M.-Y., Lee, D.-J., Tay, J.-H. & Show, K.-Y. 2007 Staining of extracellular polymeric substances and cells in bioaggregates. *Applied Microbiology and Biotechnology* **75**, 467–474.

Commenges-Bernole, N. & Marguerie, J. 2008 Adsorption of heavy metals on sonicated activated sludge. *Ultrasonics – Sonochemistry* **16**, 83–87.

Cui, K., Lau, D., Zhang, Y. & Chang, J. 2021 Mechanical properties and mechanism of nano-$CaCO_3$ enhanced sulphoaluminate cement-based reactive powder concrete. *Construction and Building Materials* **309**, 125099.

Dewil, R., Baeyens, J. & Appels, L. 2007 Enhancing the use of waste activated sludge as bio-fuel through selectively reducing its heavy metal content. *Journal of Hazardous Materials* **144**, 703–707.

He, H., Chen, Y., Li, X., Cheng, Y., Yang, C. & Zeng, G. 2017 Influence of salinity on microorganisms in activated sludge processes: A review. *International Biodeterioration & Biodegradation* **119**, 520–527.

Hong, J., Li, W., Lin, B., Zhan, M., Liu, C. & Chen, B.-Y. 2013 Deciphering the effect of salinity on the performance of submerged membrane bioreactor for aquaculture of bacterial community. *Desalination* **316**, 23–30.

Hui, W., Zhou, J. & Jin, R. 2022 Proteins recovery from waste activated sludge by thermal alkaline treatment. *Journal of Environmental Chemical Engineering* **10**, 107311.

Iizuka, A., Sakai, Y., Yamasaki, A., Honma, M., Hayakawa, Y. & Yanagisawa, Y. 2012 Bench-scale operation of a concrete sludge recycling plant. *Industrial & Engineering Chemistry Research* **51**, 6099–6104.

Iswarya, N. & Adalarasan, R. 2020 Experimental investigation on strength and durability of light weight bacterial concrete. *Materials Today: Proceedings* **22**, 2808–2813.

Kumar, A., Song, H.-W., Mishra, S., Zhang, W., Zhang, Y.-L., Zhang, Q.-R. & Yu, Z.-G. 2023 Application of microbial-induced carbonate precipitation (MICP) techniques to remove heavy metal in the natural environment: A critical review. *Chemosphere* **318**, 137894.

Liu, W., Zhao, Y., Hu, X., Li, X., Geng, Z., Wang, Q., Liu, J., Wang, H. & You, G. 2022 High performance of coal dust suppression with waste activated sludge using microbially induced calcite precipitation technology. *Powder Technology* **404**, 117464.

Ma, S., Zeng, S., Dong, X., Chen, J. & Olsson, G. 2015 Modification of the activated sludge model for chemical dosage. *Frontiers of Environmental Science & Engineering* **9**, 694–701.

Qin, J., Gong, Y., Qin, C., Meng, H., He, Y., Qin, Q. & Gao, J. 2021a $CO_2$ introduced the coagulation-flocculation of oil acidized wastewater: Pollutant removal and cost analysis. *Water Science and Technology: A Journal of the International Association on Water Pollution Research* **83** (5), 1108–1117.

Qin, J., Qin, Q., Li, X., Xue, J., Wang, R., Zhang, Q., Wang, P., Guo, Z. & Gong, Y. 2021b Urea supply control in microbial carbonate precipitation to effectively fill pores of concrete. *Construction and Building Materials* **310**, 125123.

Qin, J., Zhang, R., Yang, R. Y., Fang, J.-H., Zhang, Y., Li, X. & Gao, J. 2021c Sludge char-to-fuel approaches based on the hydrothermal fueling IV: Fermentation. *Water Science and Technology* **84** (4), 880–891.

Ramachandran, S. K., Ramakrishnan, V. & Bang, S. S. 2001 Remediation of concrete using microorganisms. *Materials Journal* **98**, 3–9.

Ramrakhiani, L., Ghosh, S., Sarkar, S. & Majumdar, S. 2016 Heavy metal biosorption in multicomponent system on dried activated sludge: Investigation of adsorption mechanism by surface characterization. In *International Conference on Advances in Bioprocess Engineering and Technology (ICABET)*, January 20–22 2016, Kolkata, India. Elsevier Science Bv, Amsterdam, pp. 3538–3552.

Raunhan, R., Jantharadej, K., Mhuantong, W., Napathorn, S. C. & Suwannasilp, B. B. 2023 Valorization of food waste derived anaerobic digestate into polyhydroxyalkanoate (PHA) using *Thauera mechernichensis* TL1. *Waste Management* **171**, 248–258.

Tian, X., Xiao, H., Li, Z., Li, Z., Su, H. & Ouyang, Q. 2022 Experimental study on the strength characteristics of expansive soils improved by the MICP method. *Geofluids* **2022**, 3089820.

Wang, S., Qu, D., Zhao, G., Yang, L., Zhu, L., Song, H. & Liu, H. 2022 Characterization of the structure and properties of the isolating interfacial layer of oil–water emulsions stabilized by soy hull polysaccharide: Effect of pH changes. *Food Chemistry* **370**, 131029.

Wilson, C. A. & Novak, J. T. 2009 Hydrolysis of macromolecular components of primary and secondary wastewater sludge by thermal hydrolytic pretreatment. *Water Research* **43**, 4489–4498.

Xuan, D., Zhan, B., Poon, C. S. & Zheng, W. 2016 Innovative reuse of concrete slurry waste from ready-mixed concrete plants in construction products. *Journal of Hazardous Materials* **312**, 65–72.

Yang, Y., Chu, J., Cao, B., Liu, H. & Cheng, L. 2020 Biocementation of soil using non-sterile enriched urease-producing bacteria from activated sludge. *Journal of Cleaner Production* **262**, 121315.

Yang, Y., Chu, J., Cheng, L. & Liu, H. 2022 Utilization of carbide sludge and urine for sustainable biocement production. *Journal of Environmental Chemical Engineering* **10**, 107443.

Yang, T., Xie, L., Hu, X., He, K., Zhu, Z., Fan, L. & Tian, W. 2023 Residual extracellular polymeric substances (EPS) detected by fluorescence microscopy on dental implants after different decontamination. *Materials Chemistry and Physics* **296**, 127242.

Yu, Z.-J., Yu, R.-L., Liu, A.-J., Jing, L., Zeng, W.-M., Liu, X.-D. & Qiu, G.-Z. 2017 Effect of pH values on extracellular protein and polysaccharide secretions of *Acidithiobacillus ferrooxidans* during chalcopyrite bioleaching. *Transactions of Nonferrous Metals Society of China* **27**, 406–412.

Zeng, Y., Chen, Z., Lyu, Q., Cheng, Y., Huan, C., Jiang, X., Yan, Z. & Tan, Z. 2023 Microbiologically induced calcite precipitation for in situ stabilization of heavy metals contributes to land application of sewage sludge. *Journal of Hazardous Materials* **441**, 129866.

Zhou, Y., Zhang, Z. Q., Zhang, J. & Xia, S. Q. 2016 New insight into adsorption characteristics and mechanisms of the biosorbent from waste activated sludge for heavy metals. *Journal of Environmental Sciences* **45**, 248–256.

First received 29 April 2024; accepted in revised form 11 July 2024. Available online 23 July 2024